Published OnlineFirst September 22, 2009; DOI: 10.1158/0008-5472.CAN-09-1482

Overactivation of the MEK/ERK Pathway in Liver Tumor Cells Confers Resistance to TGF-β–Induced Cell Death through Impairing Up-regulation of the NADPH Oxidase NOX4

Laia Caja,[1] Patricia Sancho,[1] Esther Bertran,[1] Daniel Iglesias-Serret,[2] Joan Gil,[2] and Isabel Fabregat[1,2]

[1]Laboratori de Oncologia Molecular and [2]Departament de Ciències Fisiològiques II, Institut d'Investigació Biomèdica de Bellvitge (IDIBELL), Universitat de Barcelona, L'Hospitalet de Llobregat, Barcelona, Spain

Abstract

Transforming growth factor-β (TGF-β) induces apoptosis in hepatocytes, being considered a liver tumor suppressor. However, many human hepatocellular carcinoma (HCC) cells escape from its proapoptotic effects, gaining response to this cytokine in terms of malignancy. We have recently reported that the apoptosis induced by TGF-β in hepatocytes requires up-regulation of the NADPH oxidase NOX4, which mediates reactive oxygen species (ROS) production. TGF-β–induced NOX4 expression is inhibited by antiapoptotic signals, such as the phosphatydilinositol-3-phosphate kinase or the mitogen-activated protein kinase (MAPK)/extracellular signal-regulated kinase (ERK) pathways. The aim of the present work was to analyze whether resistance to TGF-β–induced apoptosis in HCC cells is related to the impairment of NOX4 up-regulation due to overactivation of survival signals. Results indicate that inhibition of the MAPK/ERK kinase (MEK)/ERK pathway in HepG2 cells, which are refractory to the proapoptotic effects of TGF-β, sensitizes them to cell death through a mitochondrial-dependent mechanism, coincident with increased levels of BIM and BMF, decreased levels of BCL-XL and MCL1, and BAX/BAK activation. Regulation of BMF, BCL-XL, and MCL1 occurs at the mRNA level, whereas BIM regulation occurs post-transcriptionally. ROS production and glutathione depletion are only observed in cells treated with TGF-β and PD98059, which correlates with NOX4 up-regulation. Targeting knockdown of NOX4 impairs ROS increase and all the mitochondrial-dependent apoptotic features by a mechanism that is upstream from the regulation of BIM, BMF, BCL-XL, and MCL1 levels. In conclusion, overactivation of the MEK/ERK pathway in liver tumor cells confers resistance to TGF-β–induced cell death through impairing NOX4 up-regulation, which is required for an efficient mitochondrial-dependent apoptosis. [Cancer Res 2009;69(19):7595–602]

Introduction

The transforming growth factor-β (TGF-β) family plays physiologic roles during embryonic development, as well as in the control of tissue homeostasis in the adult (1). TGF-β1 is an important regulatory suppressor factor in hepatocytes, where it early inhibits proliferation (2) and induces cell death (3). However, cells that survive to its apoptotic effect (4, 5) later induce epithelial-to-mesenchymal transition, a process that mediates cell migration and survival (1, 6). Interestingly, liver tumors expressing late TGF-β–responsive genes (antiapoptotic and metastatic) display a higher invasive phenotype and increased tumor recurrence when compared with those that show an early TGF-β signature (suppressor genes; ref. 7). In this same line of evidence, blocking TGF-β up-regulates E-cadherin and reduces migration and invasion of hepatocellular carcinoma (HCC) cells (8). Indeed, any advance in the understanding of the molecular mechanisms that allow liver cancer cells to escape from TGF-β–induced apoptosis might help in future designs of targeted therapies for human HCC.

TGF-β–mediated apoptosis in hepatocytes requires the production of reactive oxygen species (ROS), which precedes the loss of mitochondrial transmembrane potential, cytochrome *c* release, and caspase activation (9, 10). We have recently described that TGF-β up-regulates the Rac-independent NADPH oxidase NOX4 in both rat and human hepatocytes, which correlates with its proapoptotic activity (11). Regulation of NOX4 occurs at the transcriptional level and is counteracted by intracellular survival signals, such as the phosphatydilinositol-3-phosphate kinase (PI3K) and the mitogen-activated protein kinase (MAPK)/extracellular signal-regulated kinase (ERK) kinase (MEK)/ERK pathways. In human HCC cell lines, NOX4 up-regulation by TGF-β is only observed in cells that are sensitive to its cytotoxic effect, such as Hep3B cells, but not in cells that are refractory to its proapoptotic effect, such as HepG2 cells. Small interfering RNA (siRNA) targeted knockdown of NOX4 in both rat hepatocytes and human Hep3B cells impairs TGF-β–induced apoptosis (11).

According to this, the aim of the present work was to analyze whether resistance to TGF-β–induced apoptosis in HCC cells might be due to impairment of the capacity of TGF-β to up-regulate NOX4 and whether or not this impairment might be due to the overactivation of survival signals that takes place in liver tumor cells.

Materials and Methods

Cell culture conditions. HepG2 human Caucasian hepatocyte carcinoma, Hep3B human Negroid hepatocyte carcinoma, and PLC/PRF/5 human liver hepatoma cells were obtained from the European Collection of Animal

Note: Supplementary data for this article are available at Cancer Research Online (http://cancerres.aacrjournals.org/).

L. Caja and P. Sancho equally contributed to this work.

Requests for reprints: Isabel Fabregat, Laboratori d'Oncologia Molecular, Institut d'Investigació Biomèdica de Bellvitge (IDIBELL), Gran Via de Hospitalet, 199, 08907 L'Hospitalet, Barcelona, Spain. Phone: 34-932-607828; Fax: 34-932-607426; E-mail: ifabregat@idibell.cat.

doi:10.1158/0008-5472.CAN-09-1482

Published OnlineFirst September 22, 2009; DOI: 10.1158/0008-5472.CAN-09-1482

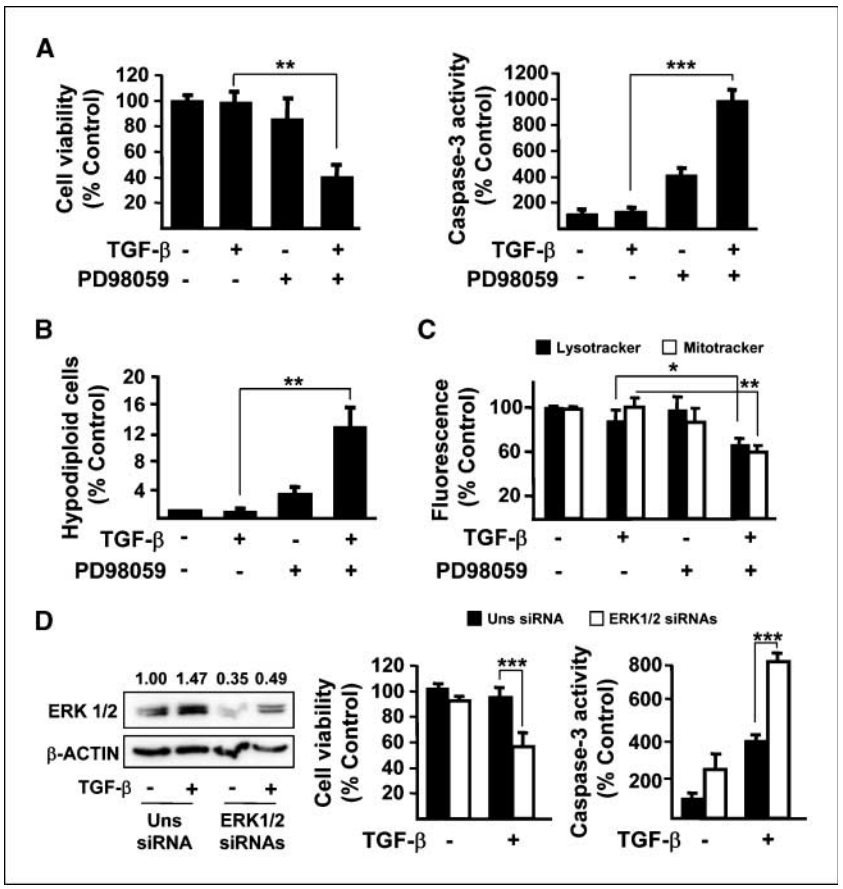

Figure 1. MEK inhibition or ERK1/2 knockdown sensitizes HepG2 cells to TGF-β–induced apoptosis. Cells were incubated in the absence or the presence of TGF-β (2 ng/mL) with or without the MEK inhibitor PD98059 (50 μmol/L). *A, left,* cellular viability (24 h of treatment); *right,* caspase-3 activity (16 h of treatment). *B,* apoptosis (24 h of treatment). *C,* analysis of lysosomal permeabilization (lysotracker) and mitochondrial transmembrane potential (mitotracker; 6 h of treatment). *D,* cells transfected with either an unsilencing (*Uns*) siRNA or specific siRNAs for ERK1 and ERK2 were treated in the absence or in the presence of TGF-β. *Left,* protein levels indicating the efficiency of targeting (16 h treatment with TGF-β). Numbers indicate densitometric analysis relative to β-actin levels. A representative experiment ($n = 3$). *Middle,* cellular viability (24 h of treatment). *Right,* caspase-3 activity (16 h of treatment). *Columns,* mean of three to six different experiments and expressed as percentage of untreated cells; *bars,* SEM. Student's *t* test: *, $P < 0.05$; **, $P < 0.01$; ***, $P < 0.001$.

Cell Cultures, cultured in MEM or DMEM supplemented with 10% fetal bovine serum (FBS), and maintained in a humidified atmosphere of 37°C, 5% CO_2. For experiments, cells at 70% confluence were serum-starved during 8 to 12 h before treatments. Treatments were as follows: PD98059 (50 μmol/L), U0126 (10 μmol/L), or PD0325901 (2 μmol/L) was added 30 min before TGF-β (2 ng/mL); glutathione-ethyl-ester (GEE, 2 mmol/L) or diphenyleneiodonium (10 μmol/L) was added 30 min before PD98059. Reagents were from Calbiochem, Cayman Chemicals, or Sigma-Aldrich.

Cell viability analysis. Cells were seeded in 96-well plate. Multitox-Fluor Multiplex Cytotoxicity Assay kit (Promega) reagents were added after treatments as indicated by manufacturer's protocol. Fluorescence was measured in a Microplate Fluorescence Reader Fluostar Optima. Viability was calculated as a ratio of live/death cells fluorescence and expressed as percentage of untreated cells.

Analysis of caspase-3 activity. Caspase-3 activity was analyzed fluorimetrically as described previously (9). Protein concentration of cell lysates was determined using the Bio-Rad protein assay kit. Results are calculated as units of caspase-3 activity per microgram of protein and expressed as percentage relative to control.

Analysis of DNA content by flow cytometry. The ploidy determination of cells was estimated by flow cytometry DNA analysis, as described previously (6).

Measurement of intracellular redox state. The oxidation-sensitive fluorescent probes 2′,7′-dichlorodihydrofluorescein diacetate (H2DCFDA; from Invitrogen) and Monochlorobimane (from Sigma) were used to analyze the total intracellular content of ROS and reduced glutathione (GSH), respectively (12). Fluorescence was measured in a Microplate Fluorescence Reader Fluostar Optima and expressed as percentage to control after correction with protein content.

Analysis of mitochondrial transmembrane potential and lysosomal permeabilization. The fluorescent probes LysoTracker Red DND-99 or MitoTracker Red CMXRos (Invitrogen) were used to fluorometrically analyze the lysosomal permeabilization and the mitochondrial transmembrane potential, respectively. Cells were detached by trypsinization, the fluorescent probes were loaded into the cells by incubation in HBSS without red phenol at a final concentration of 50 nmol/L for 30 min at 37°C and transferred in duplicate into a 96-well plate. Fluorescence was measured in a Microplate Fluorescence Reader Fluostar Optima (exc. 510, em. 590) and expressed as percentage of control after correction with protein content.

Determination of the percentage of cells containing active BAX or BAK. Cells were plated on gelatin-coated glass coverslips. The monolayer was washed with PBS, cells were fixed with 4% paraformaldehyde in PBS for 30 min at room temperature and incubated for 2 min with 0.1% Triton X-100. Primary antibodies, anti-Bax antibody 6A7 clone and anti-Bak G317-2 clone (BD Pharmingen; 1:50), were diluted in 1% bovine serum albumin and incubated for 2 h at room temperature. After several washes with PBS, the samples were incubated with fluorescent-conjugated secondary antibodies (1:200 for Alexa Fluor 488–conjugated antirabbit) for 1 h at room temperature and embedded in Vectashield with 4′,6-diamidino-2-phenylindole (DAPI) (Vector Laboratories). Cells were visualized in an Olympus BX-60 microscope with the appropriate filters. Blue signal represents the nuclear DNA staining with DAPI. Representative images were taken with a Spot 4.3 digital camera and softwared and edited in Adobe Photoshop. Results are shown as percentage of positive cells relative to cell number.

Analysis of gene expression. RNeasy Mini kit (Qiagen) was used for total RNA isolation. Reverse transcription (RT) was carried out with random primers using 1 μg of total RNA from each sample for complementary DNA synthesis. Semiquantitative PCR reactions were performed using human specific primers whose sequence is detailed in Supplementary Materials and Methods. PCR products were obtained after 30 to 35 cycles of amplification at annealing temperatures of 57 to 62°C and analyzed by 1.5% agarose gel electrophoresis. Expression of albumin was analyzed as a loading control. The RT channel contained RNA that had not been treated with the RT mixture and is shown as a specificity control. When RNA was analyzed

Published OnlineFirst September 22, 2009; DOI: 10.1158/0008-5472.CAN-09-1482

by reverse transcriptase multiplex ligation-dependent probe amplification (RT-MLPA), the SALSA MLPA KIT R011 Apoptosis mRNA from MRC-Holland (Amsterdam) for the simultaneous detection of 38 mRNA molecules was used and relative expression of each gene was normalized by β-2-microglobulin expression (13).

Western blot analysis. Total protein extracts were obtained using a lysis buffer containing 30 mmol/L Tris-HCl (pH 7.5), 5 mmol/L EDTA, 150 mmol/L NaCl, 1% Triton X-100, 0.5% sodium deoxycolate, 0.1% SDS, and 10% glycerol. Pellets were incubated during 1 h in lysis buffer at 4°C and centrifuged at 13,000 rpm during 10 min at 4°C. Western blot procedure was carried out as described previously (5). The antibodies used are detailed in Supplementary Materials and Methods.

Targeting knockdown assays. For transient siRNA transfection, cells at 70% confluence were transfected, during 8 h, using TransIT-siQuest (Mirus) at 1:300 dilution in complete medium (according to the manufacturer's recommendation). Final siRNA concentration was 25 nmol/L in NOX4 knockdown and 200 nmol/L, each one, in ERK1+ERK2 knockdown. After 16 h of incubation in complete medium, cells were trypsinized and seeded for experiments. Oligos were obtained from Sigma-Genosys. The oligo sequences were as follows:

Unsilencing: 5′GUAAGACACGACUUAUCGC 3′.
NOX4: 5′GCCUCUACAUAUGCAAUAA 3′.
ERK1: 5′UUGCGCACGUGGUCAUAGG 3′.
ERK2: 5′GUACAGGACCUCAUGGAAA 3′.

The unsilencing siRNA used was selected from previous works (14). Specific oligos with maximal knockdown efficiency were selected among three different sequences for each gene evaluated by the Dharmacon design algorithm (Thermo Fisher Scientific, Inc.-Darmachon RNAi Technologies).

Results

Inhibition of the MEK/ERK pathway sensitizes HepG2 cells to TGF-β–induced mitochondrial-dependent apoptosis. In agreement with previous results (11), HepG2 cells did not respond to TGF-β in terms of cell death (Supplementary Fig. S1*A*), although these cells responded to TGF-β inducing SMAD2 phosphorylation (Supplementary Fig. S1*B*) and mitogen-induced growth inhibition (results not shown). Among different pharmacologic kinase inhibitors, we could observe that a specific MEK inhibitor, PD98059, was able to sensitize HepG2 cells to TGF-β–induced loss of cell viability (Supplementary Fig. S1*C*). Western blot experiments revealed that HepG2 cells, cultured in the absence of FBS, showed constitutive phosphorylation of ERK (Supplementary Fig. S2*A*). This result is in agreement with previous reports indicating that HepG2 cells show alterations in the RAS pathway, which mediates overactivation of the p42/p44 MAPK (15). Other HCC cell lines that are sensitive to TGF-β–induced cell death, such as PLC/PRF-5 and Hep3B, showed much lower levels of phosphorylated ERKs activation. A correlation between ERK activation and resistance to cell death was observed (Supplementary Fig. S2*A*). Furthermore, hyperactivation of ERKs by phorbol esters in a TGF-β–sensitive cell line (Hep3B) blocked TGF-β–induced

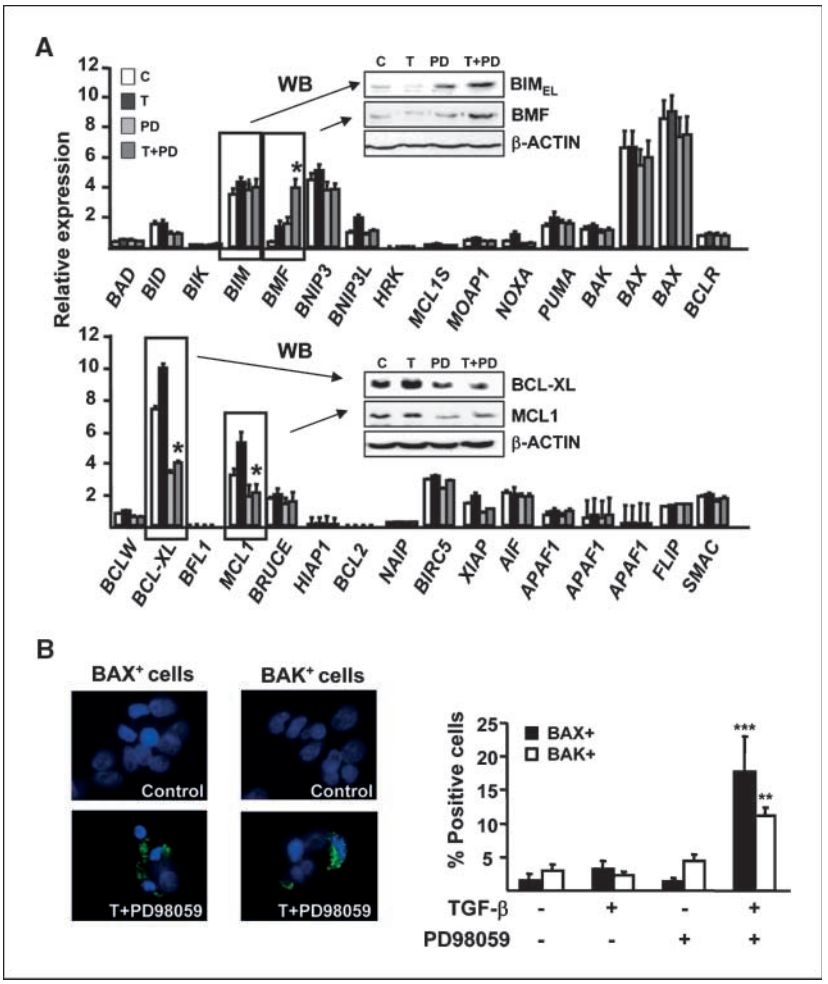

Figure 2. Combined treatment with TGF-β and PD98059 modulates the expression of different BCL-2 family members. Cells were incubated as indicated in Fig. 1 during 16 h. *A,* transcript levels of apoptotic genes by RT-MLPA. *Columns,* mean of six different experiments, expressed as fold change relative to untreated cells; *bars,* SEM. *WB,* Western blot analysis of the indicated genes. β-Actin was used as loading control; a representative experiment of 3 is shown. *B,* analysis of BAK and BAX activation by immunofluorescence. *Left,* representative photographs; *right, columns,* mean of three different experiments; *bars,* SEM. Student's *t* test versus TGF-β–treated cells: *, $P < 0.05$; **, $P < 0.01$; ***, $P < 0.001$.

Published OnlineFirst September 22, 2009; DOI: 10.1158/0008-5472.CAN-09-1482

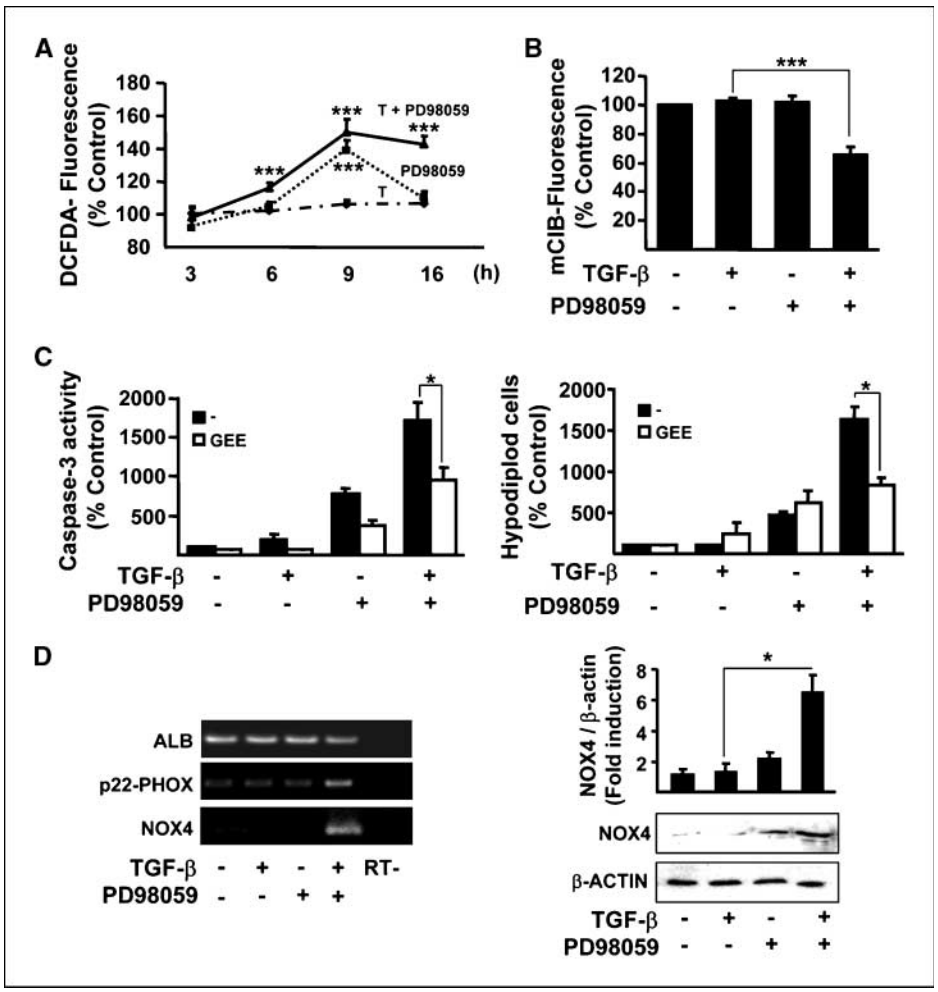

Figure 3. Combined treatment with TGF-β and PD98059 induces oxidative stress, which correlates with NOX4 up-regulation. Cells were incubated as indicated in Fig. 1. *A,* intracellular peroxide content at the indicated times of treatment. *B,* fluorimetric analysis of intracellular GSH levels (16 h of treatment). *C,* pretreatment with GEE attenuates caspase-3 activation (16 h of treatment; *left*) and apoptosis (24 h of treatment; *right*). Mean ± SEM of three independent experiments. Student's *t* test: *, $P < 0.05$; ***, $P < 0.001$. *D, left, NOX4* and *p22-PHOX* transcript levels were analyzed by RT-PCR (3 h of treatment). Albumin (*ALB*) is shown as loading control. A representative experiment is shown ($n = 3$). *Right,* NOX4 protein levels analyzed by Western blot (3 h of treatment). β-Actin is used as loading control. Densitometric analysis of three independent experiments is represented in the graph (mean ± SEM).

caspase-3 activation and apoptosis (results not shown). Interestingly, inhibition with PD98059 enhanced the cytotoxic response to TGF-β in both PLC/PRF-5 and Hep3B cells (Supplementary Fig. S2*B* and *C*). This result might be explained by the fact that TGF-β also induces antiapoptotic signals in hepatoma cells (5). Indeed, inhibition of the MEK/ERK pathway could enhance TGF-β–induced death in different HCC cells, regardless of their genetic background.

We could not observe significant differences either in SMAD2 phosphorylation or in the expression levels of different SMADs (included the inhibitory SMAD6 and SMAD7) and TGF-β receptors I and II when the MEK/ERK pathway was inhibited in HepG2 cells (Supplementary Fig. S3*A* and *B*). This result suggested that sensitization of cells to TGF-β–induced cell death might occur downstream from receptors/SMADs activation.

Exploring the potential mechanism of cell death induced by the combined treatment of TGF-β + PD98059 in HepG2 cells, we found a significant increase in caspase-3 activity and DNA fragmentation, analyzed as the percentage of cells with a DNA content lower than 2C (Fig. 1*A* and *B*), characteristic of an apoptotic process. All these events were coincident with loss of the mitochondrial transmembrane potential and the lysosomal membrane integrity, analyzed with specific fluorescent probes (Fig. 1*C*), indicating that these organelles might play a role in the mechanism of cell death. Analysis of caspase-3 in other HCC cells confirmed that MEK inhibition was enhancing TGF-β–induced apoptosis (Supplementary Fig. S2*D*). Levels of p53 did not significantly change by cell treatment with TGF-β, neither with PD98059 or the combined treatment, excluding that MEK inhibition might affect to the regulation of TGF-β on this pathway (Supplementary Fig. S3*C*). PD98059 is a specific MEK inhibitor. However, side effects could not be excluded. Therefore, we performed controls with other MEK inhibitors (Supplementary Fig. S4) and with cells where ERK1 and ERK2 expression was down-regulated with specific siRNAs (Fig. 1*D*). In all cases ERK inhibition sensitized HepG2 cells to TGF-β–induced loss in viability and activation of caspase-3, as a key regulator of apoptosis.

We next decided to focus on the molecular mechanism that might explain at which level ERK pathway is blocking TGF-β–induced apoptosis. Changes in the expression gene profile of apoptotic regulators, by using RT-MLPA, is shown in Fig. 2*A*. Transcript and protein levels of the BH3-only gene *BMF* were significantly enhanced with the combined treatment of TGF-β + PD98059. TGF-β alone up-regulated *BCL-XL* and *MCL1*, both antiapoptotic members of the BCL-2 family. However, a significant decrease in the expression of these genes was observed when the MEK/ERK inhibitor was present, which correlated with lower protein levels (Fig. 2*A*). Although we could not find variations in the expression of *BIM* at the mRNA levels, we found an increase in its protein levels when MEK/ERK was inhibited, effect that was significantly enhanced in the presence of TGF-β. In summary, the combined treatment of TGF-β and PD98059 produced an increase

Published OnlineFirst September 22, 2009; DOI: 10.1158/0008-5472.CAN-09-1482

in the levels of BIM and BMF and a decrease in BCL-XL and MCL1. This expression pattern correlated with a significant enhancement in the percentage of cells showing the active conformational form of BAX or BAK (Fig. 2*B*).

Sustained oxidative stress and significant induction of the NADPH oxidase NOX4 in TGF-β–treated HepG2 cells are observed when the MEK/ERK pathway is inhibited. In HepG2 cells, TGF-β alone was unable to induce an increase in ROS production, as analyzed with the H2-DCFDA fluorescent probe. The inhibition of MEK/ERK pathway induced a transient, although significant, increase in the intracellular ROS content, but it was the combined treatment of TGF-β and PD98059 that produced a higher and sustained intracellular ROS increase at all the examined times (Fig. 3*A*). ROS increase correlated with depletion of GSH content, which was only observed in TGF-β + PD98059–treated cells (Fig. 3*B*). Preincubation of cells with a membrane-permeable form of GSH (GEE) partially blocked the apoptotic events (Fig. 3*C*). We next wondered whether MEK/ERK inhibition might confer to HepG2 cells the capacity to respond to TGF-β in terms of NOX4 up-regulation. Results indicated that TGF-β only increased *NOX4* transcript levels in HepG2 cells when MEK/ERK were inhibited, which was coincident with the maximum expression of the NOX4 coactivator *p22-PHOX* (Fig. 3*D, left*). Interestingly, at the protein level, we might observe a slight increase in NOX4 in cells treated only with PD98059, but the highest levels were always observed with the combined treatment of TGF-β and PD98059 (Fig. 3*D, right*). It has been recently suggested that ERK activation is required for the induction of the antioxidant gene heme oxygenase-1 (HO-1) by TGF-β (16). The analysis of the levels of HO-1 revealed that TGF-β induced its expression in HepG2 cells and MEK inhibition attenuated this response (Supplementary Fig. S5). Indeed, MEK inhibition sensitizes cells to respond to TGF-β up-regulating NOX4 and impairs the up-regulation of the antioxidant gene HO-1. Other antioxidant proteins, such as catalase, Mn-superoxide dismutase, or the γ-glutamylcisteine synthetase, did not show significant changes in their levels (results not shown).

Role of NOX4 in cell death induced by the combined treatment of TGF-β and the MEK/ERK inhibitor. We next decided to target knockdown NOX4 in cells by using a siRNA approach to specifically analyze its effect on all the cell death features. NOX4 knockdown (Fig. 4*A*) decreased ROS production (Fig. 4*B*), blocked disruption of mitochondrial transmembrane potential (Fig. 4*C, left*), and significantly attenuated caspase-3 activation and the loss in cell viability induced by TGF-β + PD98059 (Fig. 4*D*). However, NOX4 knockdown did not attenuate the loss in lysosomal membrane integrity (Fig. 4*C, right*), which suggested that NOX4 was only affecting the mitochondrial-mediated mechanism of cell death. In this same line of evidence, NOX4 knockdown attenuated TGF-β + PD98059 regulation of BMF, BCL-XL, and MCL1 at the mRNA (Fig. 5*A*) and protein (results not shown) levels, and BIM at the protein level (Fig. 5*B*). Correlating with these results, NOX4 knockdown diminished the percentage of cells showing active BAX or BAK (Fig. 5*C*), suggesting

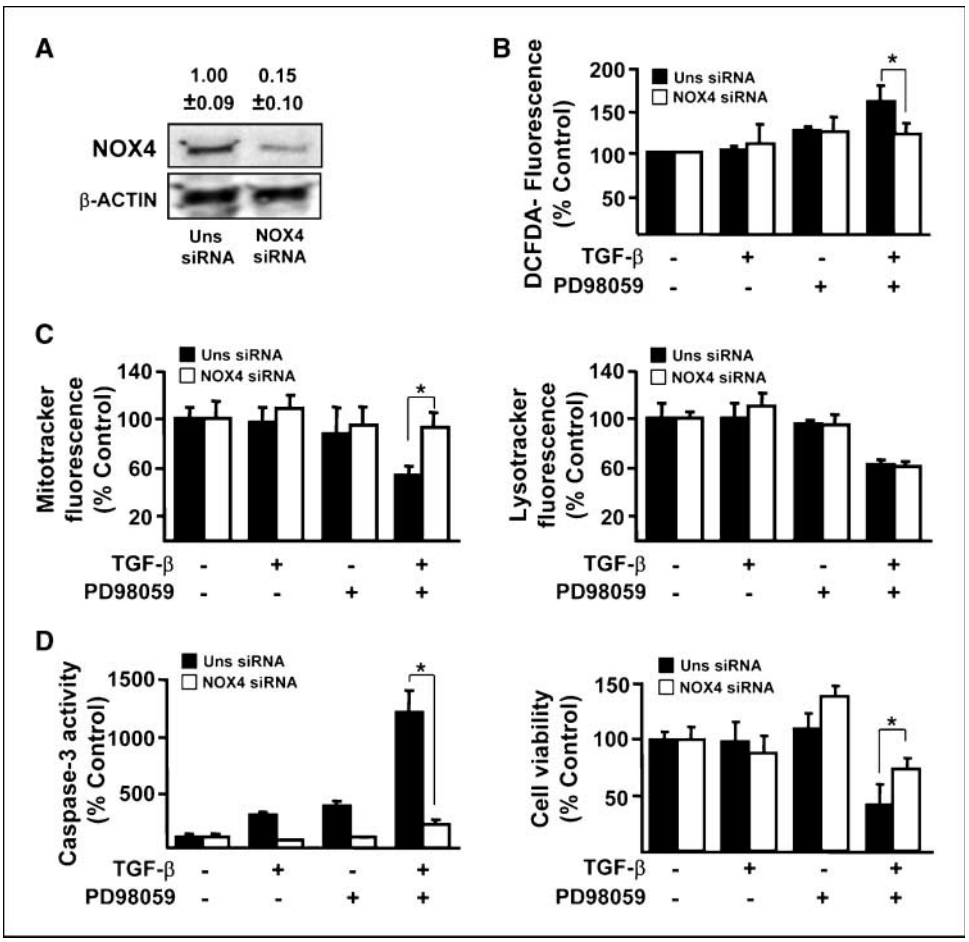

Figure 4. NOX4 targeting knockdown inhibits the mitochondrial-dependent apoptosis induced by TGF-β + PD98059. Cells transfected with either an unsilencing (*Uns*) siRNA or the specific NOX4 siRNA were treated as indicated in Fig. 1. *A,* NOX4 protein levels after 3 h of cell treatment with the combination of TGF-β + PD98059. β-Actin used as loading control. A representative experiment is shown. Mean ± SEM of densitometric analysis of three independent experiments is shown above the Western blot. *B,* intracellular peroxide content after 16 h of treatment. *C,* mitochondrial (*left*) and lysosomal (*right*) permeabilization after 6 h of treatment. *D,* caspase-3 activity after 16 h of treatment (*left*) and cell viability after 24 h of treatment (*right*). Data were calculated relative to unsilencing siRNA-tranfected untreated cells and represented as the mean ± SEM of three independent experiments in triplicate. Student's *t* test: *, $P < 0.05$.

Published OnlineFirst September 22, 2009; DOI: 10.1158/0008-5472.CAN-09-1482

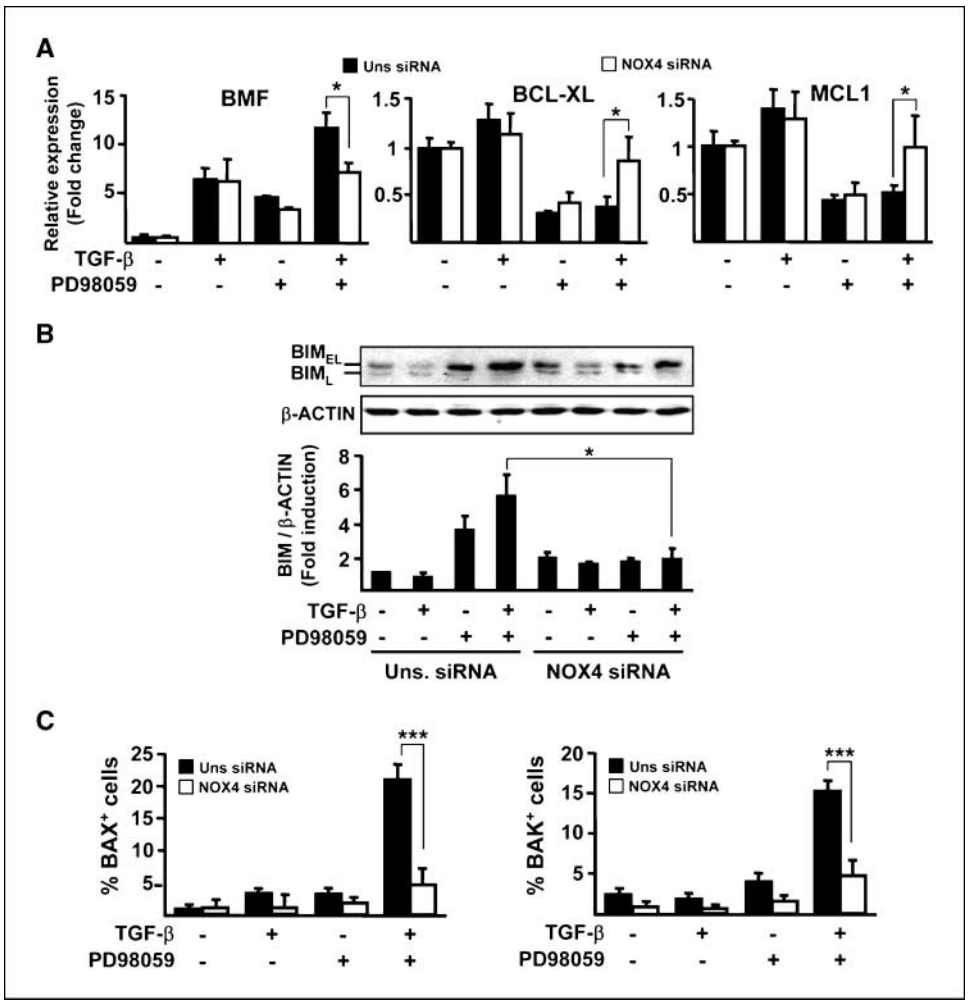

Figure 5. NOX4 targeting knockdown impairs the regulation of BCL-2 family members induced by TGF-β + PD98059. Cells were treated as indicated in Fig. 1 during 16 h. *A,* transcript levels of *BMF*, *MCL1*, and *BCL-XL* by RT-MLPA. *B,* analysis of BIM at the protein level by Western blot, β-actin used as loading control. *Top,* representative experiment; *bottom,* densitometric analysis, mean ± SEM. *C,* percentage of cells with active BAK or BAX by immunofluorescence. Data were calculated relative to unsilencing siRNA-tranfected untreated cells and represented as the mean ± SEM of three independent experiments. Student's *t* test: *, $P < 0.05$; ***, $P < 0.001$.

that NOX4 is required for TGF-β–induced mitochondrial-dependent apoptosis upstream from the regulation of BCL-2 family expression. In this same line of evidence, pretreatment of cells with a NADPH oxidase inhibitor, diphenyleneiodonium, alone or with GEE, completely blocked increase in ROS, caspase-3 activation, and regulation of the BCL-2 family genes after TGF-β + PD98059 treatment (Fig. 6).

A careful analysis of the attenuation of cell death in NOX4 targeted knockdown cells (Fig. 4*D*) revealed that a slight loss in cell viability continued being observed in response to TGF-β + PD98059. For this, we decided to explore whether or not the lysosomal permeabilization, which seemed to be NOX4 independent, might play a role in the TGF-β + PD98059–induced cell death. Among different protease inhibitors, we could only observe a slight, but significant, protecting effect on cell death with the cathepsin B inhibitor Ca-074 (Supplementary Fig. S6). These results indicate that a cathepsin B–mediated pathway might contribute to TGF-β + PD98059–induced cell death through a parallel pathway that is NOX4 independent.

Discussion

A relevant number of molecular mechanisms altered in HCC initiation and progression are compromising the balance between survival and apoptosis in the preneoplastic hepatocytes. Some physiologic proapoptotic molecules are down-regulated or inactivated in HCC, but the balance between death and survival is mainly broken due to overactivation of antiapoptotic signals (17, 18). Therefore, liver cancer cells might show stronger requirements of these intracellular pathways to survive. Alteration of RAS pathway is frequently observed in HCC, mainly due to RAS mutations and/or genetic or epigenetic silencing of inhibitors of the RAS network (19, 20), and it might confer proliferative and antiapoptotic properties to neoplastic liver cells (20). Indeed, several advances in the recent years have focused increasing attention on the role of the RAF/MEK/ERK1/2 pathway in promoting cell survival (21).

Disruption of the TGF-β suppressor arm occurs in advanced stages of HCC (7). Although some perturbations at receptor or SMAD levels have been proposed (22, 23), molecular mechanisms are not completely understood. Results presented in this manuscript indicate that overactivation of the RAS/MEK/ERK pathway in liver tumor cells might confer them resistance to the apoptotic effects of TGF-β, which is highly expressed during liver tumor progression (24). We propose that the crosstalk between ERKs and TGF-β signaling might be located on a key modulator of ROS production and intracellular oxidative stress: the NADPH oxidase NOX4, previously suggested as necessary for TGF-β–induced apoptosis in hepatocytes (11). Up-regulation of NOX4, ROS production, and oxidative stress do not occur except that MEK/ERK pathway is inhibited in HepG2 cells, which constitutively show

Published OnlineFirst September 22, 2009; DOI: 10.1158/0008-5472.CAN-09-1482

ERKs phosphorylation. NOX4 regulation by TGF-β in rat hepatocytes occurs at the transcriptional level, and it is impaired by the PI3K and MEK/ERK pathways (11). Our results confirm that a similar response must exist in humans and suggest that overactivation of survival signals in HCC cells might be counteracting TGF-β–induced cell death through attenuating NOX4 up-regulation. Interestingly, ERK activation might also contribute to the up-regulation of antioxidant genes by TGF-β, such as HO-1 (16).

Here we describe for the first time that expression of NOX4 is required for an efficient mitochondrial-dependent apoptosis by TGF-β. NOX4 is required, at least, for up-regulation of two proapoptotic BH3-only genes: *BMF* and *BIM*. It was previously reported that TGF-β transcriptionally regulates the expression of *BMF* through a ROS-dependent mechanism (25). Here we suggest that the ROS producing system involved in this process is NOX4. In the case of BIM we find that regulation occurs at a post-transcriptional level. Interestingly, it has been recently suggested that TGF-β regulates BIM by a post-translational mechanism involving SMAD-3–dependent expression of the MAPK phosphatase MKP2 (26). Our results suggest that NOX4 might mediate the regulation of MKP2 by TGF-β and overactivation of the RAS/MEK/ERK pathway in liver tumor cells would interfere with this effect. Furthermore, in HepG2 cells, as observed in fetal rat hepatocytes (4) and hepatoma cells (5), TGF-β is up-regulating antiapoptotic genes, such as the members of the BCL-2 family *BCL-XL* and *MCL1*. Interestingly, a significant decrease in the expression of these genes is observed after cell treatment with TGF-β and the MEK/ERK inhibitor, and NOX4 is required for this effect. The consequence of all these changes in the expression pattern of the BCL-2 family is an increase in the percentage of cells presenting active BAX or BAK, a decrease in the mitochondrial transmembrane potential and an activation of caspase-3, all these events being blocked when NOX4 is targeted knockdown.

During the last years, numerous articles have described the existence of NADPH oxidase homologues to the phagocytic gp91PHOX, currently named NOX2. The enzymatic activity of many of these NADPH oxidases is mainly modulated by regulatory subunits or calcium binding (27). An exception is NOX4, which seems to be independent from activators or regulatory proteins and only require p22-PHOX to be active. Thus, NOX4 activity has been described to be determined only by its mRNA/protein levels (28). NOX4 activity has been localized in intracellular membranes, such as endoplasmic reticulum (28), and preferentially originates hydrogen peroxide as a product. Upon HepG2 cell stimulation with TGF-β and the MEK/ERK inhibitor, up-regulation of NOX4 in endoplasmic reticulum might generate ROS, which would affect the correct translation/folding and/or oxidative status of different proteins, which might have consequences on transcription and translation of, at least, some apoptosis regulatory genes. Due to this intracellular localization, we wondered whether NOX4 might be affecting mechanisms of cell death promoted by other organelles, such as lysosomal-dependent events proposed for

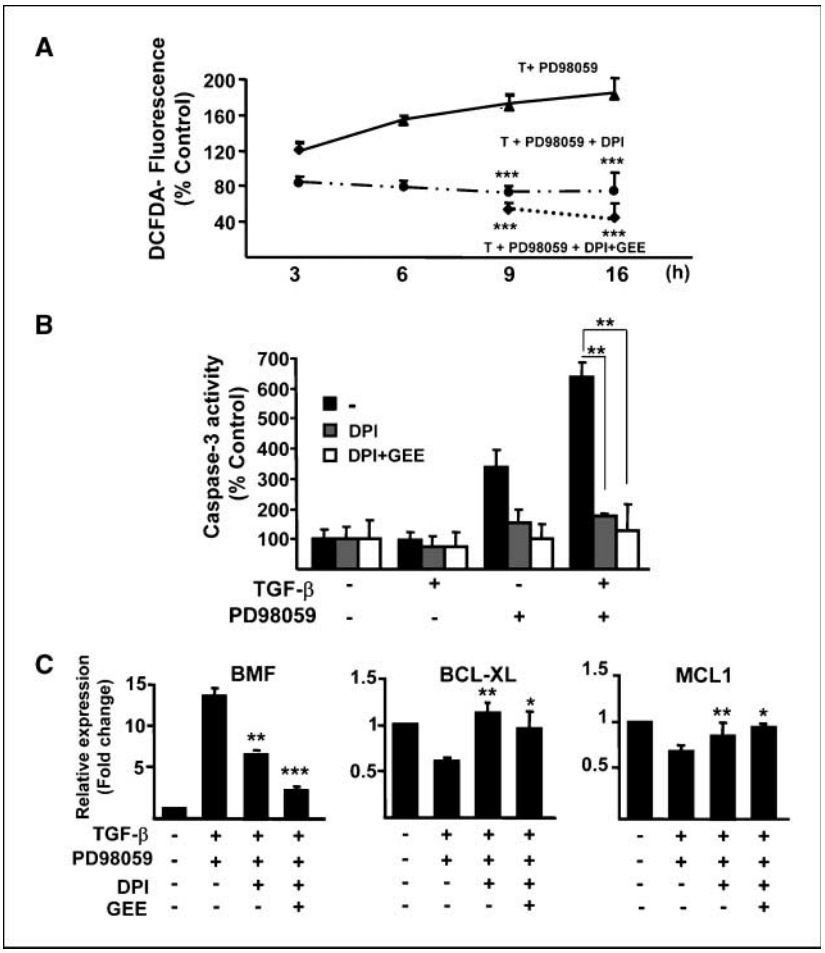

Figure 6. Oxidative stress is required for the apoptosis induced by TGF-β + PD98059. Cells were incubated as indicated in Fig. 1 and with or without diphenyleneiodonium (*DPI*, 10 μmol/L) alone or in combination with GEE (2 mmol/L), as indicated. *A,* intracellular peroxide content at the indicated times of treatment. *Points,* mean of three independent experiments in triplicate; *bars,* SEM. *B,* caspase-3 activity (16 h of treatment). *Columns,* mean of three different experiments; *bars,* SEM. *C,* transcript levels of *BMF*, *BCL-XL*, and *MCL1* after 16 h with the indicated treatments, analyzed by RT-MLPA. *Columns,* mean of three different experiments expressed as fold change relative to untreated cells; *bars,* SEM. Student's *t* test versus TGF-β + PD98059–treated cells: *, $P < 0.05$; **, $P < 0.01$; ***, $P < 0.001$.

other death-promoting factors (29). We suggest that a cathepsin B-mediated mechanism might play a role in the TGF-β–induced HepG2 cell death when MEK/ERK is inhibited, but this should be a NOX4-independent event.

In conclusion, results presented in this manuscript indicate that overactivation of the MAPK/ERK pathway in liver tumor cells might play a role in the initiation and/or development of HCC through conferring resistance to the apoptosis induced by the physiologic regulator TGF-β. As recently proposed, liver cancer stem cells might also exhibit relative resistance to TGF-β–induced apoptosis associated to up-regulation of the MAPK pathway (30). Here we show that inhibition of the MEK/ERK pathway might switch the liver tumor cell response to TGF-β, recovering the efficient signaling in terms of apoptosis and preventing other cell responses that would favor tumor progression. The key molecule in this suppressor arm should be NOX4, responsible for regulating the expression of members of the BCL-2 family, which finally govern mitochondrial-dependent events. The absence of standard systemic therapy for advanced cases of HCC has changed with the recent positive randomized trial testing the multikinase sorafenib, which represents a breakthrough in the management of this neoplasm (31). It is worthy to point out that sorafenib induces tumor cell apoptosis in HCC cells, through, at least, inhibiting the RAF/MEK/ERK pathway (32). Future work will be necessary to analyze whether these new targeted drugs might be promoting the HCC response to TGF-β in terms of apoptosis favoring tumor regression.

Disclosure of Potential Conflicts of Interest

No potential conflicts of interest were disclosed.

Acknowledgments

Received 4/22/09; revised 7/6/09; accepted 7/19/09; published OnlineFirst 9/22/09.

Grant support: Spanish Ministry of Science and Innovation [Grants BFU2006-01036 and Instituto de Salud Carlos III (ISCIII)-RTICC RD06/0020] and AGAUR-Generalitat de Catalunya grant 2005SGR-00549. L. Caja and P. Sancho are recipients of predoctoral and postdoctoral contracts, respectively, from the ISCIII, Spanish Ministry of Science and Innovation. D. Iglesias-Serret is recipient of a postdoctoral position from the José Carreras International Leukemia Foundation.

The costs of publication of this article were defrayed in part by the payment of page charges. This article must therefore be hereby marked *advertisement* in accordance with 18 U.S.C. Section 1734 solely to indicate this fact.

We thank Dr. Esther Castaño (Serveis Cientificotècnics, Institut d'Investigació Biomèdica de Bellvitge, Universitat de Barcelona) for her technical assistance in the flow cytometry and fluorimetric studies and Javier Márquez for help in editing the manuscript.

References

1. Heldin CH, Landström M, Moustakas A. Mechanism of TGF-β signalling to growth arrest, apoptosis, and epithelial-mesenchymal transition. Curr Opin Cell Biol 2009;21:166–76.
2. Carr BI, Hayashi I, Branum EL, Moses HL. Inhibition of DNA synthesis in rat hepatocytes by platelet-derived type β transforming growth factor. Cancer Res 1986;46:2330–4.
3. Oberhammer FA, Pavelka M, Sharma S, et al. Induction of apoptosis in cultured hepatocytes and in regressing liver by transforming growth factor β 1. Proc Natl Acad Sci U S A 1992;89:5408–12.
4. Murillo MM, del Castillo G, Sánchez A, Fernández M, Fabregat I. Involvement of EGF receptor and c-Src in the survival signals induced by TGF-β1 in hepatocytes. Oncogene 2005;24:4580–7.
5. Caja L, Ortiz C, Bertran E, et al. Differential intracellular signalling induced by TGF-β in rat adult hepatocytes and hepatoma cells: implications in liver carcinogenesis. Cell Signal 2007;19:683–94.
6. Valdés F, Alvarez AM, Locascio A, et al. The epithelial mesenchymal transition confers resistance to the apoptotic effects of transforming growth factor β in fetal rat hepatocytes. Mol Cancer Res 2002;1:68–78.
7. Coulouarn C, Factor VM, Thorgeirsson SS. Transforming growth factor-β gene expression signature in mouse hepatocytes predicts clinical outcome in human cancer. Hepatology 2008;47:2059–67.
8. Fransvea E, Angelotti U, Antonaci S, Giannelli G. Blocking transforming growth factor-β up-regulates E-cadherin and reduces migration and invasion of hepatocellular carcinoma cells. Hepatology 2008;47:1557–66.
9. Herrera B, Fernández M, Alvarez AM, et al. Activation of caspases occurs downstream from radical oxygen species production, Bcl-xL down-regulation, and early cytochrome *c* release in apoptosis induced by transforming growth factor β in rat fetal hepatocytes. Hepatology 2001;34:548–56.
10. Franklin CC, Rosenfeld-Franklin ME, White C, Kavanagh TJ, Fausto N. TGFβ1-induced suppression of glutathione antioxidant defenses in hepatocytes: caspase-dependent post-translational and caspase-independent transcriptional regulatory mechanisms. FASEB J 2003;17:1535–37.
11. Carmona-Cuenca I, Roncero C, Sancho P, et al. Upregulation of the NADPH oxidase NOX4 by TGF-β in hepatocytes is required for its pro-apoptotic activity. J Hepatol 2008;49:965–76.
12. Sancho P, Bertran E, Caja L, Carmona-Cuenca I, Murillo MM, Fabregat I. The inhibition of the epidermal growth factor (EGF) pathway enhances TGF-β-induced apoptosis in rat hepatoma cells through inducing oxidative stress coincident with a change in the expression pattern of the NADPH oxidases (NOX) isoforms. Biochim Biophys Acta 2009;1793:253–63.
13. Coll-Mulet L, Iglesias-Serret D, Santidrián AF, et al. MDM2 antagonists activate p53 and synergize with genotoxic drugs in B-cell chronic lymphocytic leukemia cells. Blood 2006;107:4109–14.
14. Sancho P, Fernández C, Yuste VJ, et al. Regulation of apoptosis/necrosis execution in cadmium-treated human promonocytic cells under different forms of oxidative stress. Apoptosis 2006;11:673–86.
15. Hsu IC, Tokiwa T, Bennett W, et al. p53 gene mutation and integrated hepatitis B viral DNA sequences in human liver cancer cell lines. Carcinogenesis 1993;14:987–92.
16. Churchman AT, Anwar AA, Li FYL, et al. Transforming growth factorβ-1 elicits Nrf2-mediated antioxidant responses in aortic smooth muscle cells. J Cell Mol Med 2008. "Postprint";DOI: 10.1111/j.1582–4934.2008.00636.x.
17. Mott JL, Gores GJ. Piercing the armor of hepatobiliary cancer: Bcl-2 homology domain 3 (BH3) mimetics and cell death. Hepatology 2007;46:906–11.
18. Fabregat I. Dysregulation of apoptosis in hepatocellular carcinoma cells. World J Gastroenterol 2009;15:513–20.
19. Calvisi DF, Ladu S, Gorden A, et al. Ubiquitious activation of Ras and Jak/Stat pathways in human HCC. Gastroenterology 2006;130:1117–28.
20. Calvisi DF, Pinna F, Meloni F, et al. Dual-specificity phosphatases 1 ubiquitination in extracellular signal-regulated kinase-mediated control of growth in human hepatocellular carcinoma. Cancer Res 2008;68:4192–200.
21. Balmanno K, Cook SJ. Tumour cell survival signalling by the ERK1/2 pathway. Cell Death Differ 2009;16:368–377.
22. Tang Y, Kitisin K, Jogunoori W, et al. Progenitor/stem cells give rise to liver cancer due to aberrant TGF-β and IL-6 signaling. Proc Natl Acad Sci U S A 2008;105:2445–50.
23. Yang YA, Zhang GM, Feigenbaum L, Zhang YE. Smad3 reduces susceptibility to hepatocarcinoma by sensitizing hepatocytes to apoptosis through down-regulation of Bcl-2. Cancer Cell 2006;9:445–57.
24. Luo JH, Ren B, Keryanov S, et al. Transcriptomic and genomic analysis of human hepatocellular carcinomas and hepatoblastomas. Hepatology 2006;44:1012–24.
25. Ramjaun AR, Tomlinson S, Eddaoudi A, Downward J. Upregulation of two BH3-only proteins, Bmf and Bim, during TGFβ-induced apoptosis. Oncogene 2007;26:70–981.
26. Ramesh S, Qi XJ, Wildey GM, et al. TGFβ-mediated BIM expression and apoptosis are regulated through SMAD-3-dependent expression of the MAPK phosphatases MKP2. EMBO Rep 2008;9:990–7.
27. Lambeth JD, Kawahara T, Diebold B. Regulation of Nox and Duox enzymatic activity and expression. Free Radic Biol Med 2007;43:319–31.
28. Martyn KD, Frederick LM, von Loehneysen K, Dinauer MC, Knaus UG. Functional analysis of Nox4 reveals unique characteristics compared to other NADPH oxidases. Cell Signal 2006;18:69–82.
29. Werneburg NW, Guicciardi ME, Bronk SF, Gores GJ. Tumor necrosis factor-α-associated lysosomal permeabilization is cathepsin B dependent. Am J Physiol Gastrointest Liver Physiol 2002;283:G947–56.
30. Ding W, Mouzaki M, You H, et al. CD133+ liver cancer stem cells from methionine adenosyl transferase 1A-deficient mice demonstrate resistance to transforming growth factor (TGF)-β-induced apoptosis. Hepatology 2009;49:1277–86.
31. Llovet JM, Ricci S, Mazzaferro V, et al. Sorafenib in advanced hepatocellular carcinoma. N Eng J Med 2008;359:378–90.
32. Liu L, Cao Y, Chen C, et al. Sorafenib blocks the RAF/MEK/ERK pathway, inhibits tumor angiogenesis, and induces tumor cell apoptosis in hepatocellular carcinoma model PLC/PRF/5. Cancer Res 2006;66:11851–8.

Cancer Research
The Journal of Cancer Research (1916–1930) | The American Journal of Cancer (1931–1940)

AACR American Association for Cancer Research

Overactivation of the MEK/ERK Pathway in Liver Tumor Cells Confers Resistance to TGF- β–Induced Cell Death through Impairing Up-regulation of the NADPH Oxidase NOX4

Laia Caja, Patricia Sancho, Esther Bertran, et al.

Cancer Res 2009;69:7595-7602. Published OnlineFirst September 22, 2009.